Dissociation of Difluoroethylenes. II. Direct Classical Trajectory Study of the HF Elimination from 1,2-Difluoroethylene

Jesús González-Vázquez, Emilio Martínez-Núñez,* Antonio Fernández-Ramos, and Saulo A. Vázquez

Departamento de Química Física, Universidad de Santiago de Compostela, Santiago de Compostela, E-15706, Spain

Received: August 19, 2002

Direct dynamics calculations on the HF elimination channels from cis- and *trans*-1,2-difluorotethylene (1,2-DFE) were carried out considering five different elimination mechanisms involving four-center and three-center eliminations and also H atom migrations from the cis and trans isomers. The results were compared with experimental HF vibrational state distributions and translational energy distributions at 112 and 148 kcal mol^{-1}, respectively. The calculations corroborate the experimental conclusion that direct three-center eliminations from 1,2-DFE are the major reaction pathways and take place through stepwise mechanisms in which fluorovinylidene is formed before its isomerization to fluoroacetylene. In addition, the good agreement between theory and experiment supports that the dissociation takes place through the ground electronic state.

Introduction

Among all the molecular and atomic fragmentation processes occurring in the photodissociation of difluoroethylenes (DFEs), the HF elimination is the most important one (see the first part of this work, here and after named paper I[1]). The first studies commenced 30 years ago on a series of papers that analyzed the HF vibrational state distributions.[2−5] Nowadays there is a renewed interest,[6−10] and very recently Lee and co-workers[7,8] reported the photodissociation of these molecules at 157 and 193 nm and tried to elucidate the mechanisms and dynamics of the relevant molecular processes.

Watanabe et al.[4] determined distributions of vibrationally excited HF produced by Hg-photosensitized dissociation of several fluoroethylenes. They found that 7.6% of the available energy in the products goes to HF vibrational energy in both *cis* and *trans*-DFE, and that the vibrational state distributions found for both isomers are nearly identical and near the statistical predictions, in contrast with other fluoroethylenes such as 1,1-DFE,[10] for which the HF vibrational energy content is much larger. In addition, in a previous infrared multiphoton excitation study,[5] similar HF vibrational state distributions were obtained, which suggest that direct dissociation from the electronically excited state does not take place.

Balko et al.[7] measured product translational energy distributions (TEDs) for the various product channels at 193 nm (148 kcal mol^{-1}). They found significant differences between the TED for the elimination of HF from 1,2-DFE and that for the four-center elimination from 1,1-DFE, suggesting that the exit barrier, if it exists, must be much lower than that for the four-center elimination in 1,1-DFE. They also argued that "the peaking of the TED for 1,2-DFE close to 0 kcal mol^{-1} is also evidence that the elimination is occurring from ground electronic state". They claimed that after the initial photon absorption, the electronically excited DFE must undergo internal conversion to the upper vibrational levels of the ground state from which it dissociates.

* Corresponding author. E-mail: uscqfemn@correo.cesga.es.

As detailed in paper I,[1] we found six possible pathways for HF elimination. From 1,1-DFE, the HF elimination occurs basically through channel V (see Figure 1). For this system, direct classical trajectories predict translational energy distributions and HF vibrational and rotational populations in good agreement with experiment.[10]

In the present work, we investigate the photodissociation of 1,2-DFE. Specifically, product energy distributions for HF elimination occurring through channels I−III were calculated by classical trajectories on five different semiempirical potential energy surfaces (PESs), one for each channel (channel V was already studied in a previous work[10]). Particularly, the parameters of the AM1 Hamiltonian were modified to achieve better accordance between the ab initio potential energy surface (PES) and the semiempirical AM1 calculations. This is known as AM1 with specific reaction parameters (AM1-SRP).[11] The trajectories for each channel were started from the relevant transition state structures, considering that a microcanonical ensemble is maintained at least up to the transition state region. This seems to be a good approximation since the transition states involved here are high enough to prevent the reactant from nonstatistical dynamics, at least at the energies of this study. In addition, the results extracted from the present classical trajectory results should be reliable since comparisons between classical and quantum dynamics have shown[12] that classical dynamics gives accurate results for a direct process like motion down a potential energy barrier, provided that the trajectories were initialized with the correct quasi-classical conditions. Two different excitation models were employed in this work: first, a quasi-classical normal mode rigid rotor model of Hase and co-workers[13,14] that populates the rovibrational energy levels at the barrier according to the harmonic and separable RRKM theory, and second, a modification of the efficient microcanonical sampling (EMS)[15,16] that was previously designed by our research group.[17] With this theoretical scheme, three excitation energies 100, 112, and 148 kcal mol^{-1} were selected here; the energies 112 and 148 kcal mol^{-1} are those of the experiments carried out by Watanabe et

10.1021/jp021902k CCC: $25.00
Published on Web 02/07/2003

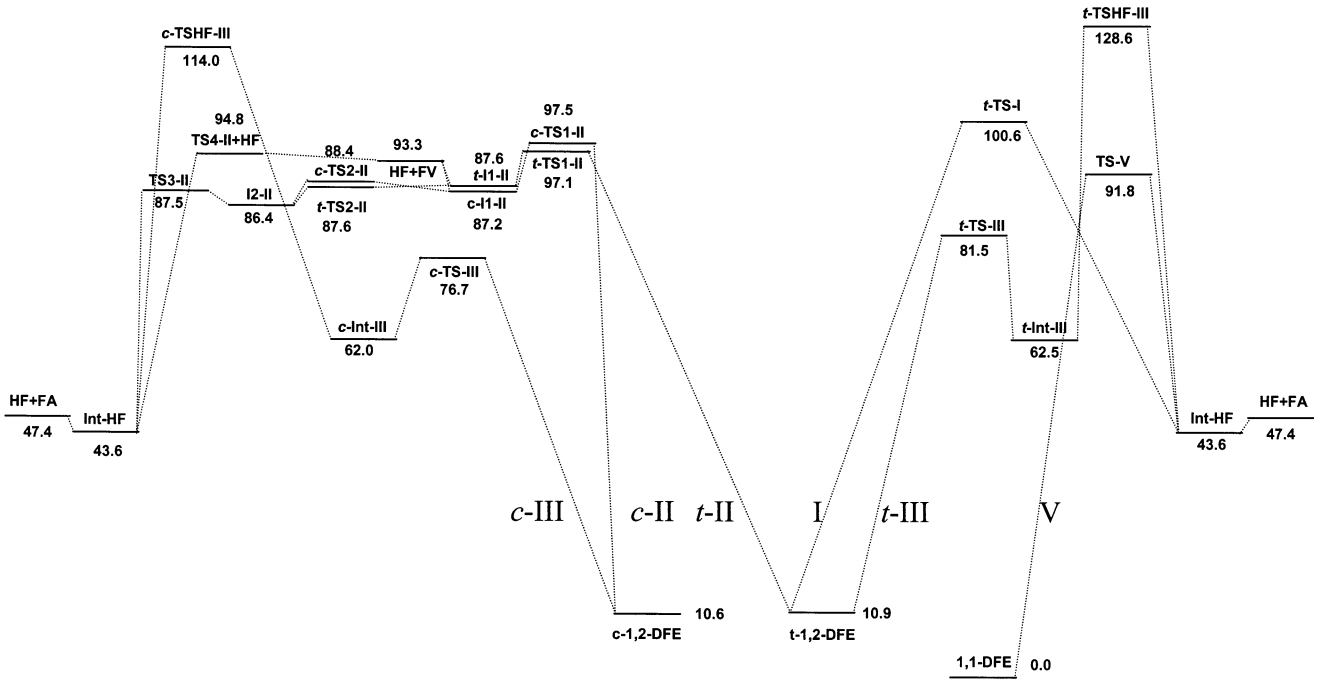

Figure 1. Schematic potential energy diagram showing the HF elimination channels involved in the 1,1-DFE and 1,2-DFE fragmentation processes.

al.[4] (herein after named exp A) and by Balko et al.[7] (herein after named exp B), respectively.

The Semiempirical Model PESs

For each channel, the AM1-SRP PES was fitted to the calculated ab initio one by minimizing a function containing structural and energetic data of the relevant stationary points for the region between the transition state and the products (HF + FA). The function employed for channel I was

$$f_{\mathrm{I}} = W_{\mathrm{E_r}}(E_{\mathrm{r}} - E_{\mathrm{r}}^{0})^2 + W_{\mathrm{F}}(\omega_{\mathrm{F}} - \omega_{\mathrm{F}}^{0})^2 \qquad (1)$$

where each term involves the AM1-SRP minus ab initio values [QCISD(T) for energies, QCISD for geometries and MP2 for frequencies; all with the 6-311G(2d,2p) basis set]. Particularly, E_{r} is the reverse barrier height for reaction (the energy difference between *t*-TS-I and the products), and ω_{F} is the imaginary frequency at the transition state *t*-TS-I. The weights in eq 1 are $W_{\mathrm{E_r}} = 1$ kcal^{-2} mol^2, and $W_{\mathrm{F}} = 5 \times 10^{-4}$ cm^2.

For channels II, we employed a similar function that reads

$$f_{\mathrm{II}} = W_{\mathrm{E}}[(E_1 - E_1^{0})^2 + (E_2 - E_2^{0})^2 + (E_3 - E_3^{0})^2 + (E_4 - E_4^{0})^2] + W_{\mathrm{F}}(\omega_{\mathrm{F}} - \omega_{\mathrm{F}}^{0})^2 + \sum_i W_{\mathrm{r}_i}(r_i - r_i^{0})^2 \qquad (2)$$

where for channel *t*-II (*c*-II), E_1, E_2, E_3, and E_4 are the relative energies between the transition state *t*-TS1-II (*c*-TS1-II) and *t*-I1-II (*c*-I1-II), I2-II and TS3-II, *t*-I1-II (*c*-I1-II) and HF + FV, and between TS1-II and the final products HF + FA, respectively (see Figure 1). Although *t*-TS2-II and *c*-TS2-II were not included in the parameterization, we verified that their relative energies with respect to the van der Waals complexes are very low, which is in agreement with the ab initio data. ω_F is the imaginary frequency at the transition state *t*-TS1-II for channel *t*-II or *c*-TS1-II for channel *c*-II, and r_i are the CF_p, CH_p, and HF_p bond distances at this transition state (H_p and F_p being the atoms of the final HF product). The weights in eq 2 are $W_{\mathrm{E}} = 1$ kcal^{-2} mol^2, $W_{\mathrm{F}} = 1 \times 10^{-3}$ cm^2, and $W_{\mathrm{r}_i} = 0.01$ Å^{-2}.

For channels III we employed the following function in the minimization procedure:

$$f_{\mathrm{III}} = W_{\mathrm{E_r}}(E_{\mathrm{r}} - E_{\mathrm{r}}^{0})^2 + W_{\mathrm{F}}(\omega_{\mathrm{F}} - \omega_{\mathrm{F}}^{0})^2 + \sum_i W_{\mathrm{r}_i}(r_i - r_i^{0})^2 \qquad (3)$$

where E_{r} is the reverse barrier, that is, the energy difference between *t*-TSHF-III (*c*-TSHF-III) and the products. The quantities ω_{F} and r_i are defined as for channels II above, but in this case they referred to transition state *t*-TSHF-III or *c*-TSHF-III. The weights in eq 3 are $W_{\mathrm{E_r}} = 1$ kcal^{-2} mol^2, $W_{\mathrm{F}} = 5 \times 10^{-4}$ cm^2, $W_{\mathrm{r_{CF}}} = 100$ Å^{-2}, $W_{\mathrm{r_{CH}}} = 4$ Å^{-2}, and $W_{\mathrm{r_{HF}}} = 1$ Å^{-2}. The weights employed in the above functions were selected to balance the importance of reverse energies, the imaginary frequency, and some selected distances at the transition state in the parameterized PES.

In paper I, a HF−FA van der Waals complex (Int-HF) was also found in the exit channel, having an energy of 3.8 kcal mol^{-1} below that of HF + FA. This complex was also found in the AM1−SRP PES with a stability of 3−4 kcal mol^{-1} (depending on the parameterization) with respect to the products, and therefore is in good agreement with the ab initio data.

Each of the five fits included 29 parameters that were optimized according to the above equations considering upper and lower bounds of ±15% of the original AM1 values. The optimized parameters for each channel are collected in Table 1. Table 2 shows a comparison between our best ab initio estimates of some attributes of the 1,2-DFE ground-state PES and those obtained with the AM1−SRP models. The maximum deviations between the ab initio and the semiempirical barriers are those involved in the energy difference between TS1-II and the products (E_4 for channel II). The other energetic differences are small. Regarding the imaginary frequencies, the comparison is very good. For distances, the major differences appear for the CF_p bond lengths. Overall, and taking into account the complexity of the global PES, the comparison between the ab initio and AM1−SRP results is satisfactory.

TABLE 1: Parameters Employed in the AM1−SRP Hamiltonians for the Five Reaction Channels of HF Elimination from 1,2-DFE

parameter	channel I	channel *t*-II	channel *c*-II	channel *t*-III	channel *c*-III
U_{ss} (H)	−11.016000	−11.472403	−11.366037	−10.256784	−10.290889
β_s (H)	−6.800000	−6.173787	−6.461897	−5.568168	−6.190250
Z_s (H)	1.187840	1.116793	1.069270	1.169596	1.140555
α (H)	2.901539	2.651738	2.882324	2.882324	2.882324
G_{ss} (H)	12.848000	12.762347	12.848000	12.419733	13.224874
U_{ss} (C)	−52.028658	−49.253796	−52.028658	−52.028658	−52.028658
U_{pp} (C)	−39.614239	−38.293764	−39.614239	−39.614239	−39.614239
β_s (C)	−15.715783	−15.401467	−15.715783	−16.668625	−15.715783
β_p (C)	−7.719283	−7.530589	−7.575189	−8.251056	−7.733986
Z_s (C)	1.828000	1.989531	1.808665	1.986563	1.808665
Z_p (C)	1.685116	1.685116	1.685116	1.741287	1.685116
α (C)	2.648274	2.789515	2.648274	2.507033	2.701239
G_{ss} (C)	12.230000	11.985400	12.230000	12.835762	12.230000
G_{sp} (C)	11.470000	10.475933	11.470000	12.158200	11.470000
G_{pp} (C)	11.080000	11.080000	11.080000	9.972000	11.109547
G_{p2} (C)	10.561600	9.840000	9.840000	10.561600	10.299200
H_{sp} (C)	2.430000	2.326320	2.430000	2.274660	2.492846
U_{ss} (F)	−149.732000	−122.495021	−136.105579	−136.105579	−136.105579
U_{pp} (F)	−104.889885	−100.694290	−104.889885	−104.889885	−104.889885
β_s (F)	−69.590277	−69.590277	−69.590277	−70.054212	−69.590277
β_p (F)	−27.922360	−25.688571	−27.922360	−27.922360	−27.922360
Z_s (F)	3.770082	3.996287	3.895751	3.644413	3.770082
Z_p (F)	2.494670	2.611088	2.494670	2.295096	2.494670
α (F)	5.517800	5.113161	5.517800	5.395183	5.517800
G_{ss} (F)	16.916000	15.228000	16.920000	18.612000	16.920000
G_{sp} (F)	17.250000	15.755000	15.525000	15.525000	15.525000
G_{pp} (F)	16.041600	16.407629	16.821400	16.599834	17.147821
G_{p2} (F)	14.214200	13.916000	14.910000	14.910000	14.910000
H_{sp} (F)	4.830000	5.130533	4.830000	4.368548	4.830000

TABLE 2: Some Attributes of the ab Initio and AM1−SRP PESs[a]

	channel I		channel *t*-II		channel *c*-II		channel *t*-III		channel *c*-III	
	ab initio	AM1-SRP	ab initio	AM1-SRP	ab initio	AM1-SRP	ab initio	AM1-SRP	ab initio	AM1-SRP
E_r	53	53					81	78	67	66
E_1			10	10	10	14				
E_2			1	0.4	1	0.2				
E_3			6	5	6	7				
E_4			50	57	50	56				
F	1928	1972	1198	1198	1265	1261	1899	1846	1496	1539
r_{CF}	1.81	1.68	1.86	2.32	1.83	2.13	1,91	1.98	1.87	1.96
r_{CH}	1.43	1.56	1.26	1.36	1.26	1.28	1.15	1.27	1.15	1.27
r_{HF}	1.14	1.15	1.14	1.28	1.13	1.28	1.39	1.38	1.43	1.43

[a] Energies in kcal mol^{-1}, frequencies in cm^{-1} and distances in Å.

Trajectory Computational Details

The trajectories were initiated at transition states *t*-TS-I, *t*-TS1-II, *c*-TS1-II, *t*-TSHF-III, and *c*-TSHF-III, which are associated to channels I, *t*-II, *c*-II, *t*-III and *c*-III, respectively, by using two sampling methods. The first is a quasi-classical rigid rotor/normal mode (hereinafter named QRR/NM), described in detail elsewhere,[13,14] which allows one to obtain a microcanonical ensemble of rovibrational states at the barrier by assigning n_i, J, K quanta to a given degree of freedom, using the following probability function

$$P(n_i,J,K) = \frac{N^{ts}_{n_i,J,K}}{N^{ts}_{tot}} \qquad (4)$$

where N^{ts}_{tot} is the total number of rovibrational states at the barrier and $N^{ts}_{n_i,J,K}$ is the barrier sum of states with a given degree of freedom having a fixed number of quanta. Two specific cases were considered in this study. First, a sampling over the vibrational states with $J = 0$ [QRR/NMv], and second, taking into account J and K in the sampling [QRR/NMvJK]. In the latter method, quantum numbers n_i, J, and K were sampled according to eq 4; further details are given in ref 10.

The other barrier sampling employed here is based on the EMS method of Nyman, Nordholm, and Schranz,[15,16] which takes into account the full anharmonicity and vibrational coupling of the potential energy surface. In this procedure a Markov chain is constructed by randomly moving some (or all) of the Cartesian coordinates of our system with the sampling confined to a specific part of the phase space. If the sampling is carried out in the reactant region, most of the (internal) coordinates are naturally bound by energetic considerations. However, if the sampling is carried out at the transition state, care must be taken with some coordinates associated with the reaction coordinate mode, since one may be sampling regions that do not belong to the dividing surface. Very recently,[17] the EMS at the barrier was employed by propagating the Cartesian coordinates in the direction of the $3N-7$ normal modes perpendicular to the reaction coordinate (this sampling will be hereinafter named EMSNM). It should be pointed out that Nyman et al.[18] used a similar sampling for the water molecule using internal coordinates (the two distances and the angle). In these cases one needs to know the Jacobian for the transformation, which should be included in the weighting factor for uniformly sampling the molecular phase space.[16,19] In our case, the Jacobian for the transformation (from Cartesian to normal

TABLE 3: Vibrational Populations of HF Obtained in the Five Reaction Channels of HF Elimination from 1,2-DFE at an Excitation Energy of 112 kcal mol^{-1} [a]

		channel I			channel *t*-II		channel *c*-II		channel *t*-III		channel *c*-III		total[b]	
v	exp A[a]	QRR/NMv	EMS	EMSNM	QRR/NMv	EMSNM	QRR/NMv	EMSNM	QRR/NMv	EMSNM	QRR/NMv	EMSNM	QRR/NMv	EMSNM
1	1.00	1.00	1.00	1.00	1.00	1.00	1.00	1.00	1.00	1.00	1.00	1.00	1.00	1.00
2	0.21	0.45	0.54	0.49	0.27	0.36	0.34	0.34	1.93	0.96	0.70	0.46	0.32	0.37
3	0.11	0.09	0.20	0.16	0.04	0.14	0.06	0.04	1.62	0.71	0.34	0.31	0.06	0.11
4	0.06	0.03	0.07	0.07	0.00	0.06	0.00	0.00	0.55	0.33	0.17	0.16	0.01	0.04
f_{vib}	7.6	10.0	14.9	13.5	5.1	6.3	5.9	3.3	31.8	27.4	16.4	15.9	6.1	6.2

[a] Experimental results of Watanabe et al.[4] [b] Total vibrational populations calculated as a weighted contribution from the five channels studied here and channel V reported in ref 10.

mode coordinates $\mathbf{Q} = \mathbf{Lq}$) is just $|\mathbf{L}|^{-1}$, which is a constant and therefore the weighting factor is the same as in the EMS for $J = 0$. This method is only approximate, since the normal mode eigenvectors are only valid for small displacements from the transition state region. For high excess energies at the barrier, and therefore large displacements from the equilibrium transition state structure, the reaction coordinate is no longer separable from the remaining degrees of freedom. However, we will show how the EMSNM gives results in very good agreement with EMS, with the advantage that can be used at the barrier in a straightforward way.

In the present work, we employed this EMSNM procedure to prepare a microcanonical ensemble of molecules at each of the transition states. In addition, and to compare the reliability of our sampling, for channel I a conventional EMS was carried out at the barrier. The approximation followed here to set up the phase space boundaries in the EMS is the same used in a previous classical trajectory study of 1,1-DFE.[10] Briefly, the boundaries for the combination of some geometrical parameters in the QRR/NMv sampling were recorded first, and then used to define the configuration space limits of the transition state.

For each channel, we considered three energies 100, 112, and 148 kcal mol^{-1} above the zero point vibrational energy (ZPVE) of the reactant, except for channel *t*-III, for which only the two higher energies were selected because 100 kcal mol^{-1} is below the *t*-TSHF-III energy. Thus, employing the above-mentioned excitation models QRR/NMv, QRR/NMv*JK*, EMSNM, and EMS (only for channel I), we designed a total of 45 ensembles comprising 2000 trajectories each.

The trajectories were integrated with a fourth order Runge−Kutta routine and a step size of 0.05 fs, using an extensively adapted version of the GENDYN program [D. L. Thompson, GENDYN program], which incorporates the relevant subroutines of MOPAC7.0.[20,21] During the integration of the trajectories, energy conservation of better than four digits was obtained. When the HF−FC≡CH center-of-mass distance reached 10 Å, the trajectories were halted and product internal and relative translational energies were computed.

Results and Discussion

A. HF Vibrational Populations. Table 3 collects the vibrational state distributions obtained in this work at an excitation energy of 112 kcal mol^{-1} with the different excitation models and for the five elimination channels. The differences found here between the four-center (I) and the three-center (II) channels, which are the more important among all the molecular elimination channels (see paper I), may be attributed to differences in the corresponding pathways. Channel I presents a large reverse barrier for HF elimination (53 kcal mol^{-1}), part of which is converted to vibrational energy of HF. It should be noticed that these vibrational state distributions obtained for channel I are very similar to those for 1,1-DFE at the same energy,[10] for which basically only the four-center elimination takes place. Specifically, for 1,1-DFE we obtained a percentage of available energy of 11−13 going to HF vibration, which is similar to that predicted here for the four-center elimination from *trans*-1,2-DFE (10−15 kcal mol^{-1}). This suggests that the four-center HF eliminations in 1,1-DFE and 1,2-DFE are very similar to each other.

Channels II show small exit barriers for HF elimination, as depicted in Figure 1 [the energy difference between *c*-TS1-II (*t*-TS1-II) and HF + FV is 4.3 (3.8) kcal mol^{-1}]. Note that HF is formed in the first elementary step, which leads to the HF−FV van der Waals complex *c*-I1-II (*t*-I1-II). As detailed in paper I, the above intermediate may dissociate or evolve on a flat region of the PES (through I2-II) toward products. We thought it to be of interest to investigate the relative importance of these two reaction paths, even though the HF vibrational state distributions should not differ significantly from each other. For this purpose we run a batch of trajectories from the cis isomer with EMSNM at an excess energy over the barrier of 8 kcal mol^{-1}, which is below the energy of the TS4−II transition state with our AM1-SRP potential. Therefore, all trajectories leading to FA must necessarily go through TS3-II. Under these conditions we did not find trajectories arriving at FA, indicating that the formation of HF + FV is virtually the only path that takes place, which is in agreement with the suggestions of Balko et al.[7]

Finally, for the least frequent channels III, which implies an initial H migration between the carbon atoms and a subsequent three-center HF elimination, the vibrational state populations indicate that HF is highly excited in comparison with the other mechanisms. This can be explained by the stretched HF distances at the corresponding transition states (about 1.4 Å) in comparison with the equilibrium bond length (0.9 Å) in the HF molecule. Quantum-mechanically, this corresponds to a high Franck−Condon projection of the transition state wave function onto the product HF wave function for high vibrational levels.[22]

B. Translational Energy Distributions. Figure 2 displays graphically the TEDs obtained here for each of the channels I, *t*-II, *c*-II, *t*-III, and *c*-III [panels a−e in the figure, respectively]. For channel *t*-III at 148 kcal mol^{-1}, the EMSNM results are not listed because the low number of reactive trajectories found for this case makes the statistics unreliable. Channels I and III have very large reverse barriers. As a consequence, the fragments rapidly dissociate with considerable translational energy, having little chance to randomize the available energy at the barrier, which results in nonstatistical product energy distributions. By contrast, for channels II a partial redistribution of energy may take place in the exit channel since the reverse barriers are small. In particular, the TEDs for channels I and III peak at energies between 20 and 30 kcal mol^{-1}, whereas those for channels II peak between 5 and 10 kcal mol^{-1}, which is closer to the statistical predictions. For sake of comparison,

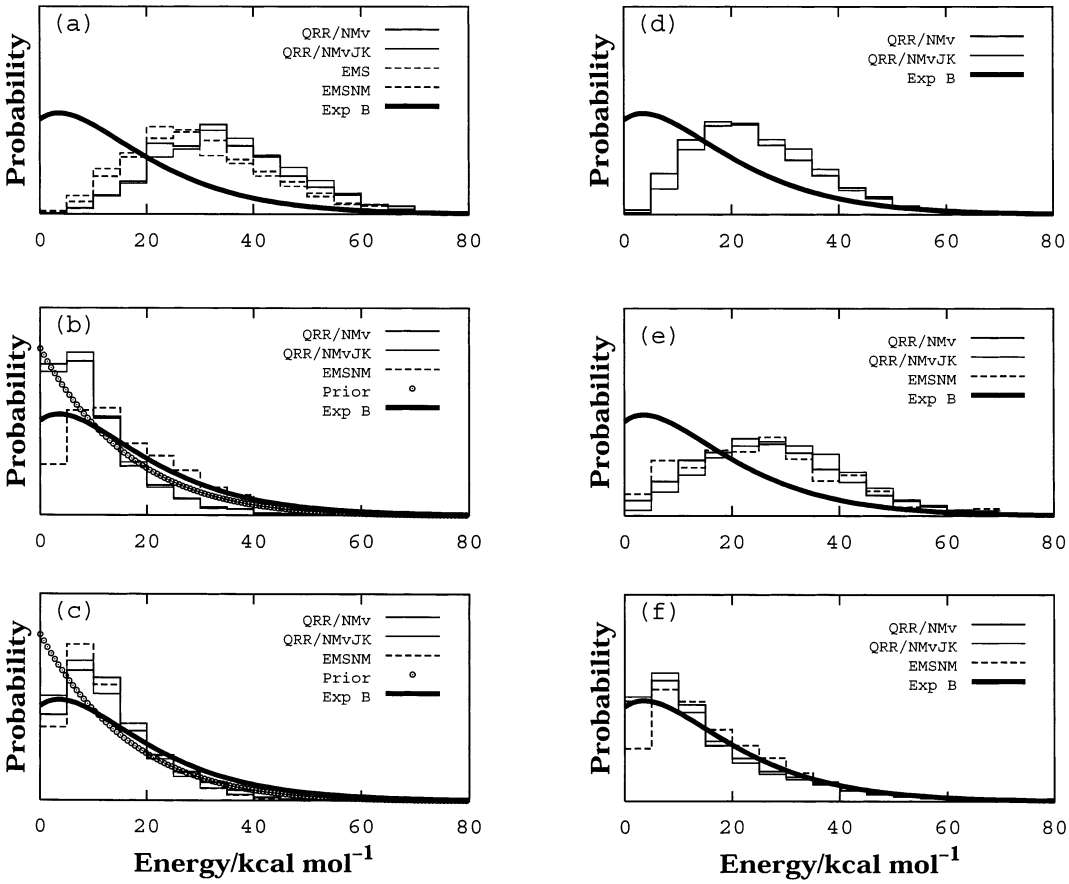

Figure 2. Translational energy distributions for (a) channel I, (b) channel *t*-II, (c) channel *c*-II, (d) channel *t*-III, (e) channel *c*-III, and (f) averaged results at 148 kcal mol^{-1} (193 nm) of excitation energy. The thick line corresponds to the experimental results of Balko et al.[7]

we also calculated prior distributions[23,24] for channels II. The resulting distributions are shown in Figure 2 [panels b and c] and compared with the trajectory results. As shown in this figure, the prior distributions (dot circles) are in moderately good agreement with the classical trajectory results. The prior distributions peak at 0 (it has the general shape of a two-dimensional canonical translational energy distribution), whereas the classical trajectory distributions peak between 5 and 10 kcal mol^{-1}. The presence of a small reverse barrier may be a source of discrepancy, although the inclusion of the conservation of angular momentum in the statistical calculation might lead to a distribution in closer agreement with the trajectory results.

C. Variation of the Product Energy Distributions with Excitation Energy. The average translational energies E_{trans} obtained in this work for the different channels and excitation models (QRR/NMv and EMSNM) are depicted in Figure 3 as a function of the available energy E_{av}. Following the "sum rule" proposed by Zamir and Levine,[25] the translational energy can be expressed as a contribution from the reverse barrier E_b and a contribution from the excess energy $E_{av} - E_b$

$$E_{trans} = aE_b + b(E_{av} - E_b) \quad (5)$$

where a and b are constant values. The above equation means that the two components of the available energy are both partly converted into translational energy, but with different efficiencies, which are measured by the coefficients a and b.

We determined the fractions of reverse barrier and excess energy a and b that go to product translation by least-squares fittings of the average translational energy to eq 5 (obviously, this makes more sense in the case of channels I and III; however we included the values for all the channels for completeness). The resulting values are listed in Table 4. For the nonstatistical channels (I and III), a high percentage of the exit barrier is converted to product translation (between 26% and 62%). Most of the reverse barrier energy in the nonstatistical channels goes to product translation and HF vibrational energy. On the other hand, the percentage of excess energy partitioned to translational energy is low (between 2% and 15%) for channels I and II. Considering that only the reaction coordinate energy goes to product translation, the percentage a should be 8.33% (1 over $3N - 6$). The differences might be attributed to the initial energy

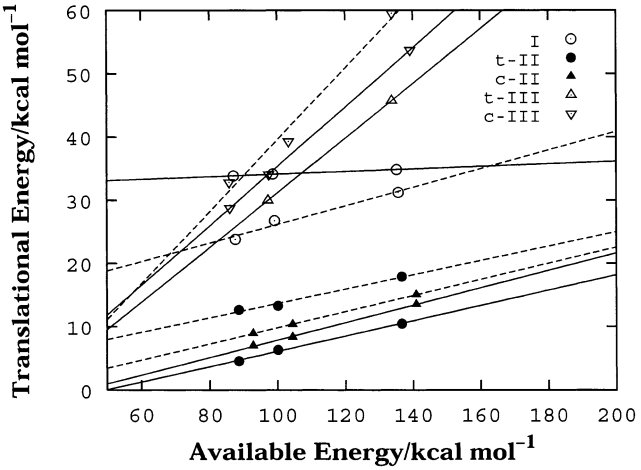

Figure 3. Correlation between translational energy and available energy for the five HF elimination channels. Solid lines are the least-squares fitting for the QRR/NMv excitation models, and the dashed lines are those for EMSNM.

TABLE 4: Least-Square Fittings to Eq 5

channel	excitation model	parameter *a*	parameter *b*
I	QRR/NMv	0.62	0.02
	EMS	0.37	0.13
	EMSNM	0.36	0.15
t-II	QRR/NMv	0.02	0.12
	EMSNM	0.15	0.11
c-II	QRR/NMv	0.03	0.13
	EMSNM	0.08	0.12
t-III	QRR/NMv	0.28	0.43
c-III	QRR/NMv	0.29	0.47
	EMSNM	0.26	0.56

content in the disappearing modes, which correlate with product translations and rotations. In addition, a portion of the energy in the reaction coordinate mode is converted into product rotation. The very large percentage of the excess energy converted to product translation for channel III (between 43 and 56%) seems to indicate that most of the vibrational modes (including the disappearing modes) at the transition state are highly coupled to the reaction coordinate.

In addition, we should remark that the values in Table 4 are only rough estimates due to the uncertainty in the average values, the use of only three points in the fitting, and the possibility of a nonlinear relationship between the average translational energy and the available energy in the whole energy range.[26]

Table 5 shows that, for all excitation energies, the energy content of FA is substantially higher for channels II than for channel I. Particularly, for the lowest energy selected here, the energy content of FA is about twice larger for channels II. As the excitation energy increases, the excess energy also increases, and therefore the percentage of the reverse barrier height (over the total available energy) becomes increasingly less important. In addition, the rotational energies for the four-center and three-center channels are very similar within each excitation model, indicating that probably the percentage of exit barrier that goes to rotation in the products for channel I is not very high.

Finally, channels III are the most nonstatistical among all, since they concentrate most of the available energy in product translation and rotations and in HF vibrational energy, with very little vibrational energy content in the FA molecule. This may arise from a substantial coupling between the transition state vibrational modes and product translational and rotational degrees of freedom. The high vibrational energy content of HF was also explained above on the basis of the stretched HF distance at the transition state.

D. Comparison Between the Results of the Different Excitation Models. The vibrational state distributions collected in Table 3 and the TEDs of Figure 2 for channel I with EMS are in very good agreement with those obtained with EMSNM. For this channel, which is highly nonstatistical, the EMS and EMSNM translational energy distributions peak at lower energies than the QRR/NM distributions [see Figure 2a]. The main reason for this discrepancy arises from the separability of the reaction coordinate inherent to the QRR/NM models.[10,27] In the EMS Hamiltonian the reaction coordinate is not separable and has kinetic and potential couplings with the remaining modes. This leads to an initial average reaction coordinate energy in the EMS-type ensembles substantially lower than that in QRR/NM. As a result, if the channel is nonstatistical, the product translational energies may be shifted to lower values. However, if a significant fraction of the excess energy is converted to product translation, the above trend may not hold. This is what we found for channels III, where the EMSNM product translational energies are higher than those obtained with QRR/NM sampling.

For channels II, the EMSNM distributions peak at energies slightly higher than those obtained with QRR/NM sampling. These channels present a transition state looser than that for the four-center channel and are more statistical. Therefore, a mechanism of vibrational−translational energy transfer may be taking place in the course of the elimination, and since the initial vibrational energy content is higher in the EMSNM ensembles, this transfer should be more effective for the EMSNM-initialized trajectories than for those initialized by QRR/NM sampling. This vibrational−translational energy transfer is expected to be less acute from the cis isomer (*c*-II), since the translational energy distributions are in this case more similar.

Finally, the results for TEDs (see Figure 2) and vibrational state distributions under QRR/NMv ($J = 0$) excitation are very similar to those obtained with QRR/NMvJK, which indicates that the effects of rotational motion on the computed product energy distributions are not important.

E. Comparison with Experiment. Table 3 also shows the vibrational population of product HF molecules and the fraction of available energy that goes to HF vibration obtained by

TABLE 5: Product Energy Partitioning Obtained in the Five Reaction Channels of HF Elimination from 1,2-DFE[a]

	channel I			channel *t*-II		channel *c*-II		channel *t*-III		channel *c*-III	
	QRR/NMv	EMS	EMSNM	QRR/NMv	EMSNM	QRR/NMv	EMSNM	QRR/NMv	EMSNM	QRR/NMv	EMSNM
						$E = 100$ kcal mol^{-1}					
E_{trans}	39	28	27	5	14	8	10			34	38
$E_{rot,HCCF}$	7	8	7	5	9	5	6			9	11
$E_{vib,HCCF}$	37	36	36	76	53	74	73			21	9
$E_{rot,HF}$	4	10	11	4	11	4	4			15	11
$E_{vib,HF}$	13	18	19	10	13	9	7			21	31
						$E = 112$ kcal mol^{-1}					
E_{trans}	35	24	27	6	13	8	10	31	30	35	40
$E_{rot,HCCF}$	7	8	8	7	9	6	6	7	8	10	10
$E_{vib,HCCF}$	38	39	38	72	57	71	71	32	28	20	14
$E_{rot,HF}$	6	11	10	5	10	5	5	11	11	13	10
$E_{vib,HF}$	14	18	17	10	11	10	8	19	23	22	26
						$E = 148$ kcal mol^{-1}					
E_{trans}	26	22	23	8	13	10	11	34		40	44
$E_{rot,HCCF}$	8	7	7	8	8	7	7	8		9	9
$E_{vib,HCCF}$	43	44	44	66	58	65	66	29		18	18
$E_{rot,HF}$	8	12	12	7	10	7	7	11		12	9
$E_{vib,HF}$	15	16	15	11	11	11	9	18		21	20

[a] Percentage over the total available energy.

Watanabe et al.[4] (exp A) at an excitation energy of 112 kcal mol^{-1}. They found that 7.6% of the available energy goes to HF vibrational energy, which is between the values calculated for channel I (10.0−14.9) and channels II (3.3−6.3). It should be noticed that the fraction obtained here was calculated with respect to the ZPVE of the products to make a direct comparison with experiment. For vibrational levels above $v = 1$, the calculations predict a better agreement with experiment for channels II than for channel I, especially for the vibrational quantum number distribution obtained for channel *t*-II with the EMSNM excitation model. This suggests that channels II are the most probable mechanisms for HF elimination at 112 kcal mol^{-1}, which supports the experimental conclusions.

Taking into account the RRKM calculations reported in paper I, the relative yields (in percentage) of HF for channels I: (*t*-II: *c*-II: *t*-III: *c*-III: V) are 10.1: 49.2: 37.9: 0.0: 0.1: 2.7 at 112 kcal mol^{-1} (the energy of exp A) and 13.5: 41.7: 39.2: 0.2: 2.0: 2.5 at 148 kcal mol^{-1} (the energy of exp B). At the energy of exp A channels II are 4−5 times more probable than channel I and about 400 times than channel *c*-III (channel *t*-III is classically forbidden at this energy). At the energy of exp B these ratios are somewhat lower but still substantial. Combining the RRKM branching ratios and the vibrational state populations of all channels (the values for channel V are taken from ref 10), we obtained the total (averaged) vibrational populations, which show, in general, better agreement with exp A than do the results for each individual channel.

The calculations obtained for channels I and III [Figure 2, panels a, d, and e, respectively] predict TEDs that peak between 20 and 30 kcal mol^{-1}, whereas the experimental curve[7] peaks at $\sim$ 8 kcal mol^{-1}. The calculated distributions for channels II, especially that of EMSNM for channel *t*-II, are in much closer agreement with that obtained by Balko et al.[7] (exp B) than are those calculated for the other channels. This corroborates their conclusion that the three-center elimination through channels II is the most important mechanism in the photodissociation of 1,2-DFE. When the above RRKM branching ratios are used to construct a TED that accounts for all channels studied here (including the four-center elimination from 1,1-DFE[10]), the distributions shown in Figure 2f are obtained. As shown in this plot, the agreement between the combined trajectory+RRKM results and exp B is very good for all the excitation models, especially for the QRR/NM ensembles. Finally, the good agreement between the theoretical and experimental results also supports that HF elimination takes place in the ground-state PES.[7]

Conclusions

In this work, product energy distributions were obtained for the HF elimination from 1,2-DFE by direct AM1−SRP trajectory calculations. The trajectories were run from the transition states to the products for five dissociation channels. The product energy distributions calculated for these channels showed significant differences among them. Particularly, the four-center and H atom migration mechanisms are highly nonstatistical, with a large percentage of the reverse barrier going to product translational energies, whereas the three-center eliminations through channels II are more statistical. In fact, comparisons between statistical calculations and our classical trajectory results on the TEDs show reasonable agreement. The calculations also indicated that the direct three-center eliminations (channels II) lead to HF + FV (i.e., 1,2-DFE → HF + FA is stepwise), which agrees with the experimental interpretation.[7]

The comparison between theoretical and experimental vibrational state populations and translational energy distributions corroborates that channels II constitute the main HF elimination mechanism and that the dissociation takes place in the ground electronic state.

Acknowledgment. E.M.-N. and S.A.V. thank Ministerio de Ciencia y Tecnología of Spain for financial support (Project BQU2000−0462). E.M.-N. and A.F.-R. also thank the above ministry for their Ramón y Cajal research contracts.

References and Notes

(1) González-Vázquez, J.; Fernández-Ramos, A.; Martínez-Núñez, E.; Vázquez, S. A. *J. Phys. Chem. A* **2003**, *107*, 1389.
(2) Strausz, P. O.; Norstrom, R. J.; Salahub, D.; Gosavi, R. K.; Gunning, H. E.; Csizmadia, I. G. *J. Am. Chem. Soc.* **1970**, *92*, 6395.
(3) Clough, P. N.; Polyanyi, J. C.; Taguchi, R. T. *Can. J. Chem.* **1970**, *48*, 2919.
(4) Watanabe, H.; Horiguchi, H.; Tsuchiya, S. *Bull. Chem. Soc. Jpn.* **1980**, *53*, 1530.
(5) Quick, C. R., Jr.; Wittig, C. *J. Chem. Phys.* **1980**, *72*, 1694.
(6) Hall, G. E.; Muchermann, J. T.; Presses, J. M.; Weston, R. E., Jr.; Flynn, G. W.; Persky, A. *J. Chem. Phys.* **1994**, *101*, 3679.
(7) Balko, B. A.; Zhang, J.; Lee, Y. T. *J. Phys. Chem. A* **1997**, *101*, 6611.
(8) Lin, J. J.; Wu, S. M.; Huang, D. W.; Lee, Y. T.; Yang, X. *J. Chem. Phys.* **1998**, *109*, 10838.
(9) Lin, S.-R.; Lee, Y.-P. *J. Chem. Phys.* **1999**, *111*, 9233.
(10) Martínez-Núñez, E.; Estévez, C. M.; Flores, J. R.; Vázquez, S. A. *Chem. Phys. Lett.* **2001**, *348*, 81.
(11) González-Lafont, A.; Truong, T.; Truhlar, D. G. *J. Phys. Chem.* **1991**, *95*, 4618.
(12) Untch, A.; Schinke, R.; Cotting, R.; Huber, J. R. *J. Chem. Phys.* **1993**, *99*, 9553.
(13) Doubleday, C.; Bolton, K.; Peslherbe, G. H.; Hase, W. L. *J. Am. Chem. Soc.* **1996**, *118*, 9922.
(14) Bolton, K.; Hase, W. L.; Peslherbe, G. H. *Modern Methods for Multidimensional Dynamics in Chemistry*; World Scientific: Singapore, 1998.
(15) Nyman, G.; Nordholm, S.; Schranz, H. W. *J. Chem. Phys.* **1990**, *93*, 6767.
(16) Schranz, H. W.; Nordholm, S.; Nyman, G. *J. Chem. Phys.* **1991**, *94*, 1487.
(17) Martínez-Núñez, E.; Vázquez, S. A.; Varandas, A. J. C. *Phys. Chem. Chem. Phys.* **2002**, *4*, 279.
(18) Nyman, G.; Rynefors, K.; Holmlid, L. *J. Chem. Phys*. **1988**, *88*, 3571.
(19) Peslherbe, G. H.; Wang, H.; Hase, W. L. *Adv. Chem. Phys.* **1999**, *105*, 171.
(20) Stewart, J. P. P.; MOPAC 7.0, a General Molecular Orbital Package QCPE, 1993; p 455.
(21) Stewart, J. P. P. *J. Comput. Chem.* **1989**, *10*, 209.
(22) Mourdaunt, D. H.; Osborn, D. L.; Neumark, D. M. *J. Chem. Phys.* **1998**, *108*, 2448.
(23) Levine, R. D.; Kinsey, J. L. *Atom-Molecule Collision Theory−A Guide for the Experimentalist*; Plenum: New York, 1979.
(24) Baer, T.; Hase, W. L. *Unimolecular Reaction Dynamics*; Oxford University Press: New York, 1996.
(25) Zamir, E.; Levine, R. D. *Chem. Phys.* **1980**, *52*, 253.
(26) Lorquet, J. C. *J. Phys. Chem. A* **2000**, *104*, 5422.
(27) Martínez-Núñez, E.; Vázquez, S. A. *J. Phys. Chem. A* **2001**, *105*, 4808.